Mutagenesis, 2018, 33, 333–340
doi:10.1093/mutage/gey019
Original Manuscript

Original Manuscript

A novel *FAM83H* mutation in one Chinese family with autosomal-dominant hypocalcification amelogenesis imperfecta

Shunlan Yu[1], Junkang Quan[1], Xiaozhe Wang[1], Xiangyu Sun[1], Xianli Zhang[1,2], Yang Liu[1], Chenying Zhang[1,*] and Shuguo Zheng[1,*]

[1]Department of Preventive Dentistry, Peking University School and Hospital of Stomatology, National Engineering Laboratory for Digital and Material Technology of Stomatology, Beijing Key Laboratory of Digital Stomatology, Beijing, PR China and [2]Department of Stomatology, Xuanwu Hospital Capital Medical University, Beijing, PR China

*To whom correspondence should be addressed. Tel: +86 10 82195510; Fax: +86 10 62173402; Email: zhengsg86@gmail.com, Tel: +86 10 82195558; Email: zhangchy168@163.com

Received 23 April 2018; Revised 16 July 2018; Editorial decision 16 July 2018; Accepted 24 July 2018.

Abstract

Autosomal-dominant hypocalcification amelogenesis imperfecta (ADHCAI) is characterized by soft enamel that easily disintegrates and exposed dark dentin. ADHCAI is caused by mutations in a gene called family with sequence similarity 83 member H (*FAM83H*). To investigate the molecular genetics of ADHCAI, a Chinese family in which three generations exhibited ADHCAI was recruited. The enamel ultrastructure was analysed by environmental scanning electron microscopy (ESEM), which showed altered enamel rod (prism) structures in ADHCAI patients compared to the structures in healthy controls. Mutational analysis of the *FAM83H* gene identified a novel nonsense mutation (c.1222A>T) in the affected family members that encodes a stop codon at amino acid position 408, causing premature protein truncation (p. K408X). Green fluorescent protein (GFP) and FAM83H fusion protein analyses *in vitro* showed that normal cytoplasmic accumulation of the FAM83H protein was prevented by the K408X mutation in both rat dental epithelial SF2 cells and human embryonic kidney 293T cells. The mutant fusion protein localized primarily to the nucleus, in contrast to the cytoplasmic subcellular localization of the wild-type FAM83H protein. Our results provide new genetic evidence that mutations in *FAM83H* contribute to ADHCAI.

Introduction

Amelogenesis imperfecta (AI) is a genetic disease affecting tooth enamel formation. It can occur as an isolated entity or as a phenotype of some syndromes, including enamel–renal syndrome and Jalili syndrome, and the prevalence varies from 1:700 to 1:14,000 based on the studied populations (1). Although AI is heterogeneous in aetiology as well as in phenotype, it can be categorized into three main types: hypoplastic, hypocalcified and hypomatured (2). Clinically, the enamel in the hypoplastic type exhibits reduced thickness but is often hard and translucent (3); whereas hypomatured enamel has a mottled, discoloured appearance and can be easily chipped (4). Hypocalcified AI is the most severe form, which is characterized by malformed, easily disrupted enamel after tooth eruption due to extreme softness; the remaining surfaces appear rough and discoloured (5). Distinctive changes in enamel structure are observed during the development of each type of AI (6).

Dental enamel is an epithelial-derived tissue containing highly organized hydroxyapatite crystals (HA; $Ca_{10}[PO_4]_6[OH]_2$) and is formed by ameloblasts during tooth development. Amelogenesis requires the secretion of a proteinaceous matrix in which immature enamel HA crystallites are deposited. The matrix is then degraded and almost entirely replaced by HA mineral. Amelogenesis is described in three functional stages: the pre-secretory, secretory and maturation stages (3). In the pre-secretory stage, ameloblasts acquire distinctive properties and generate a synthetic protein apparatus to secrete the organic enamel matrix. During the secretory

phase, ameloblasts secrete the entire enamel thickness. Throughout the maturation stage, organic materials and water are removed, and the enamel is converted into the hardest tissue in the human body by the continuous deposition of phosphate and calcium (7,8).

The classification of AI is correlated with the stages of enamel formation (6). Defects in the secretory stage result in insufficient crystal elongation, generating a pathologically thin enamel layer and thereby leading to hypoplastic AI. Hypomineralized AI is caused in the maturation stage when ameloblasts produce an enamel layer of normal thickness that is pathologically soft. The hypomineralized phenotype can be further subdivided into hypomaturation and hypocalcification. Hypomaturation is caused by incomplete removal of protein from the enamel matrix, whereas hypocalcification is characterized by the insufficient transport of calcium ions (Ca2+) into the developing enamel, thus leading to soft enamel.

The entire process of amelogenesis is genetically controlled and is well regulated by proteins with various functions, including the enamel matrix proteins (AMELX, AMBN, ENAM) and the proteases that degrade them (MMP20, KLK4). In addition, cell–cell and cell–matrix adhesion molecules (ITGB6, LAMA3, LAMB3, COL17A1, AMTN, and FAM83H) and transport proteins (WDR72 and SLC24A4) also play important roles during the process of amelogenesis (6). It has been shown that each type of AI is caused by genetic changes in specific genes, each of which can exhibit different modes of inheritance, such as X-linked or autosomal dominant. For instance, hypoplastic AI without systemic conditions is caused by mutations in the *AMELX* gene in an X-linked pattern (9) or by mutations in *ENAM, LAMB3* (10), or *AMBN* (11) in an autosomal pattern. Mutations in *MMP20, KLK4* (12), *WDR72* (13) and *SLC24A4* (14) are associated with hypomaturation AI with an autosomal pattern of inheritance, and hypocalcified AI is mainly associated with defects in the *FAM83H* gene.

Defects in the *FAM83H* gene are most widely reported in autosomal-dominant hypocalcified AI (ADHCAI) cases (6). The *FAM83H* gene encodes a protein containing 1179 amino acids, of which approximately 80% are encoded by exon 5, the final exon (15). To date, 30 mutations in *FAM83H* are reported to cause ADHCAI in different populations. All of the mutations identified are located in the last and largest exon, exon 5, and except for two missense mutations, all of the mutations are nonsense or frameshift variants predicted to cause premature translation termination (6). MRNAs that encode premature translation termination in the final coding exon generally escape nonsense-mediated decay (16).

One three-generation Chinese family with ADHCAI diagnoses was recruited for this study, which investigated a potentially novel mutation of the *FAM83H* gene and its impact on protein function in ADHCAI patients.

Material and methods

Subjects

A Chinese family exhibiting ADHCAI in three generations was recruited. The proband was a 20-year-old man who complained that his teeth were aesthetically impaired. His medical history revealed no health concerns or allergies. Clinical and radiologic examinations resulted in ADHCAI diagnosis according to the clinical diagnostic criteria (3). Oral examinations were performed on all of his family members. Five normal, healthy age- and gender-matched controls were also enrolled. Written informed consent from the participants or guardians of the minors was obtained for all participants. This study was ethically approved by the Ethical Committee of Peking University School and Hospital of Stomatology (issue number: PKUSSIRB-201631124).

Mutation analysis

Peripheral blood samples were obtained from normal controls and the patient's family members (eight affected and three non-affected individuals). Genomic DNA was extracted from peripheral blood using the TIANamp Blood DNA mini kit (Tiangen, Beijing, China) according to the manufacturer's instructions. The entire coding region and adjacent intron boundaries of the *FAM83H* gene were amplified by polymerase chain reaction (PCR) using conditions and primers described previously (17). The amplification products were assessed by 2% agarose gel electrophoresis and purified with a PCR purification kit (Omega, Norcross, GA) according to the manufacturer's instructions. Purified PCR products were bi-directionally sequenced using an ABI 3730 XL automatic sequencer (Applied Biosystems, Foster City, CA). DNA sequences were analysed using NCBI databases and the BLASTN (BLAST nucleotide) program (http://blast.ncbi.nlm.nih.gov/).

Prediction of damaging effects

To predict if the mutation is disease-causing, we used the online program Mutation Taster (http://www.mutationtaster.org). The secondary structures of the wild-type and mutant FAM83H proteins were predicted using the online program PSIPRED Protein Sequence Analysis Workbench (http://bioinf.cs.ucl.ac.uk/psipred/).

Histological analysis

For the histological analysis of AI-affected teeth, two third molars were extracted from the proband, sectioned and examined using environmental scanning electron microscopy (ESEM, Quanta 200F, FEI, America). Two teeth were donated voluntarily by healthy individuals of similar ages who were not related to the family and were used as controls. The extracted teeth were sectioned using EXAKT systems (300CP, EXAKT, Germany) after embedding in epoxy resin. Specimens were etched with 37% phosphoric acid for 10 seconds and washed with copious amounts of water for 20 s. Specimens were analysed with ESEM under 15 kV.

Mutagenesis of expression vectors

The pEGFPC1-FAM83H plasmid (kindly provided by Prof. Jan C-C. Hu, Department of Biologic and Materials Sciences, University of Michigan School of Dentistry) expressing the wild-type human FAM83H protein was used, as previously described (5). The mutation to create the amino acid substitution (c.1222A>T, p. K408X) was introduced using Quick-Change Lightning Site-Directed Mutagenesis Kit (Agilent Technologies, Cedar Creek, TX) according to the manufacturer's protocol. All of the plasmids were completely sequenced to exclude random mutagenesis.

Cell culture and transient transfection

Human embryonic kidney 293T cells (HEK-293T) and rat dental epithelial SF2 cells (RDE-SF2) (kindly provided by Prof. Fukumoto Satashi, Department of Oral Health and Development Sciences, Tohoku University Graduate School of Dentistry) were used in our study. The cells were cultured at 37 °C in humidified air containing 5% CO_2. HEK-293T cells were cultured in Dulbecco's modified Eagle's medium (DMEM, Life Technologies Corporation, Grand Island, NY) supplemented with 10% foetal bovine serum (FBS, Life Technologies Corporation). RDF-SF2 cells were cultured in

DMEM-F12 medium supplemented with 10% FBS, and 1% penicillin and streptomycin (Life Technologies Corporation) was added to both media.

Plasmid DNA for the pEGFP-C1 vector expressing GFP, as well as pEGFP-C1 expressing wild-type or mutant FAM83H fused to GFP, was used for transient transfection. HEK-293T cells and RDF-SF2 cells were trypsinized, counted, and seeded onto a microscope cover glass in 12-well plates at a density of 5×10^4 cells per well. After overnight incubation, 1 μg of plasmid DNA was transfected into HEK-293T cells using 1.5 μl of Lipofectamine 3000 (Thermo Fisher, Beijing, China) according to the manufacturer's instructions. One microgram of plasmid DNA was also transfected into RDF-SF2 cells with 2 μl Lipofectamine LTX. Duplicate slides were seeded for each transfection.

Subcellular localization assay

Twenty-four hours after transfection, the cells were washed three times (5 min each wash) with phosphate-buffered saline (PBS) and then fixed with 4% paraformaldehyde for 15 min. After three 5-min washes with PBS, the coverslips were mounted with 4′,6-diamidino-2-phenylindole (DAPI)-containing mounting medium (ZLI-9557, ZSGB-BIO, Beijing, China). Cells were visualized and captured using the Zeiss LSM 5 EXCITER confocal

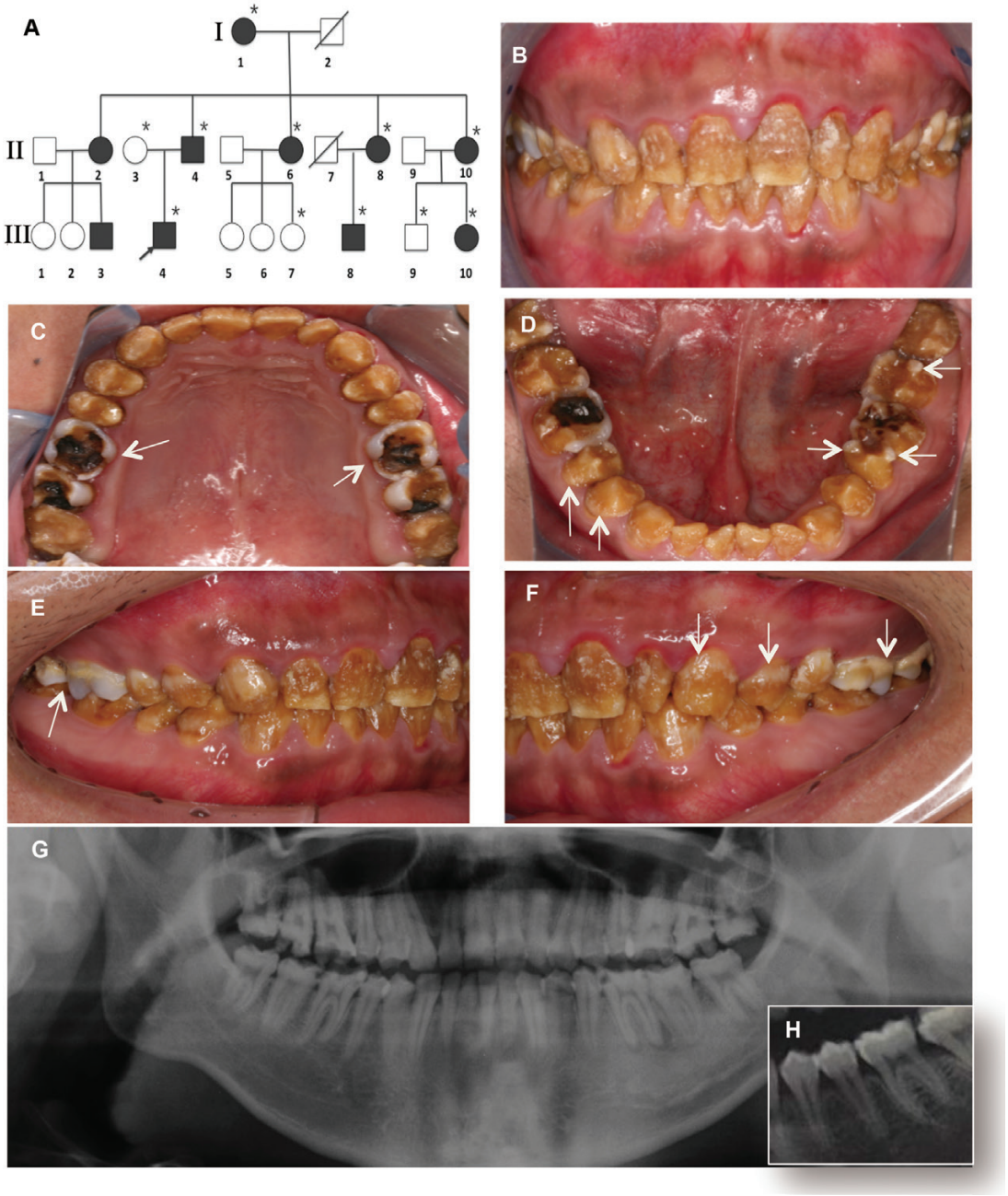

Figure 1. Clinical and radiographic phenotype of the proband with ADHCAI. (**A**) Pedigree of the family. Asterisks (*) indicate members recruited for this study. Males are marked as squares and females as circles. Filled symbols designate affected individuals; open symbols indicate those not affected. The black arrow is the proband. Symbols with a slash signify a deceased family member. (**B**–**F**) Intraoral photographs of the proband (III: 4). Extensive discolouration and loss of enamel was seen. Small focal islands of normal-looking enamel were found in the cusp and/or cervical area (white arrows). (**G**) Panoramic radiograph of the proband showed that the density of the enamel was reduced and exhibited a similar radiographic manifestation to the underlying dentin. Insert box shows the density of normal teeth matched by age and gender matched to the proband.

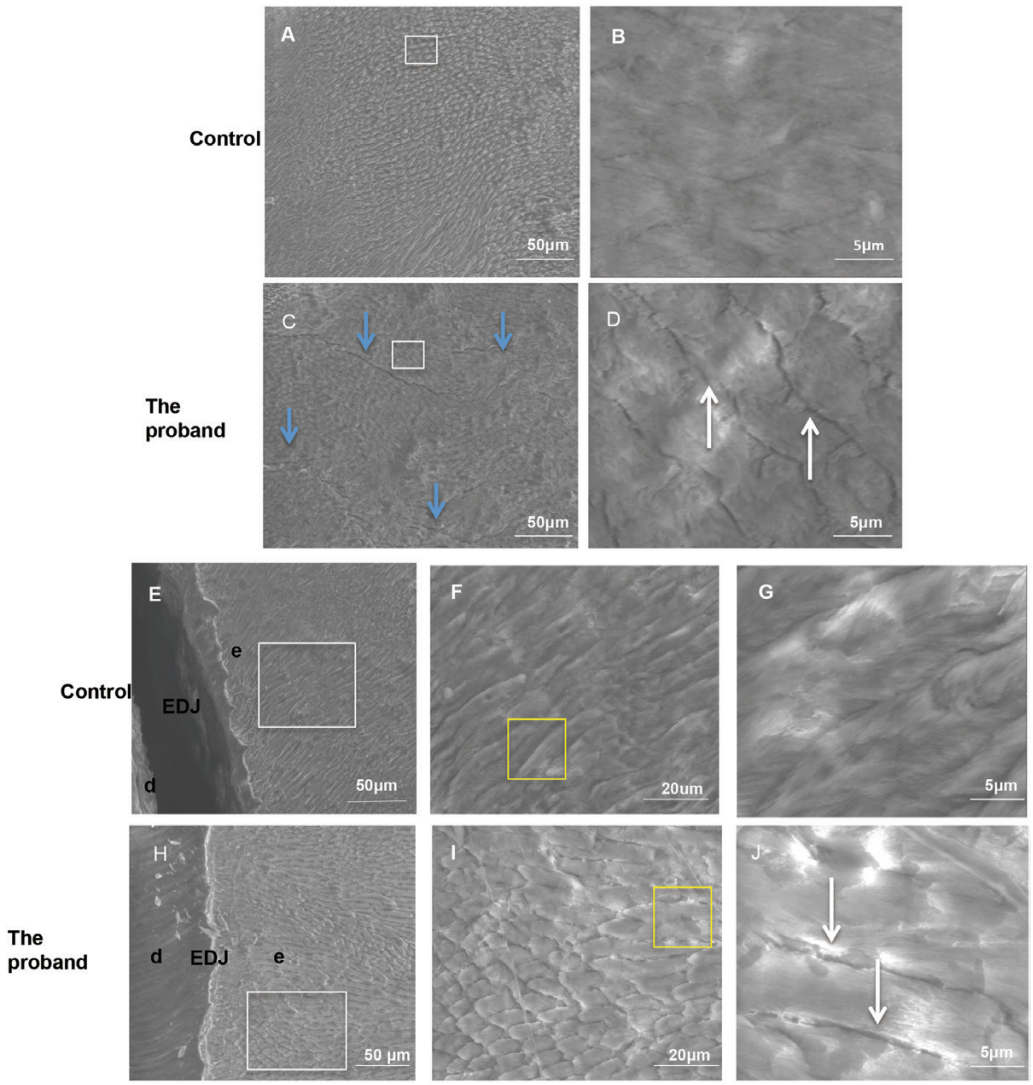

Figure 2. Ultrastructure of enamel in the proband. Representative images collected with environmental scanning electron microscopy of normal control (**A**, **B**, **E–G**) and proband (**C**, **D**, **H–J**) enamel in a cross-section view (A–D) and a vertical-section view (E–J). The enamel layer of affected permanent teeth was a poorly formed prismatic structure with cracks or crevices (the gray arrows in C), and the interspace of the enamel rods was widened (the white arrows). B, D, F and I are magnified images for the areas in A, C, E and H that are circled by white boxes. G and J are magnified images for the areas in F and I that are circled by white boxes. EDJ: enamel-dentinal junction; e: enamel; d: dentin.

microscope (Carl Zeiss, Jena, TH, Germany). The experiment was performed in triplicate.

Results

Clinical findings

This study focused on a 20-year-old male patient with a typical hypocalcified AI phenotype. His pedigree contained 22 family members and exhibited an autosomal-dominant pattern of inheritance (Figure 1A). The medical history of the family members revealed no significant systematic disease, allergy or use of medication. Therefore, ADHCAI was diagnosed for this family based on the clinical findings and the pattern of inheritance.

The dental malformation of the proband was primarily soft and easily disintegrated enamel and exposed dark dentin with brown and black discolouration (Figure 1B–F). The enamel was exfoliated from most of the teeth, causing reduced crown height (Figure 1C and D). Some small zones of normal enamel thickness were observed along the gingival margin (Figure 1D and F). In some molars, the tip of the cusps appeared normal and intact (Figure 1C and D). However, in areas with an intact enamel surface, the enamel was usually opaque and chalky (Figure 1E and F). The patient did not have an anterior open bite (Figure 1B). The panoramic radiograph of the proband showed enamel loss and a reduced radiodensity distinction between the enamel and dentin compared to normal teeth (Figure 1G).

Ultrastructure of the enamel

The ultrastructure of the enamel in the proband was analysed by ESEM. Clear differences were observed in the enamel prism structure between the control (Figure 2A and B and E–G) and the proband (Figure 2C and D and H–J). The enamel of the normal control exhibited well-defined prism structures and compact prism/interprism continuas (Figure 2A and B and E–G). In contrast, the enamel layer of the proband showed prismatic structures with cracks or crevices (Figure 2C and D). The enamel prism was poorly formed, and the interprismatic gap was increased (Figure 2D and J). Furthermore, the direction of enamel rods in the proband was abnormal (Figure 2H).

Mutation analysis

To identify mutations in the *FAM83H* gene in ADHCAI patients, we analysed the coding region. DNA fragments from exon 1 to exon 5 of the *FAM83H* gene were amplified by genomic PCR and directly sequenced. A heterozygous c.1222A>T mutation was detected in exon 5 of the *FAM83H* gene in the proband (Figure 3A). This novel mutation introduces a stop codon at amino acid position 408, leading to a prematurely truncated protein (p. K408X) that is 772 amino acids shorter than the wild-type protein (Figure 3B). Consistent with its phenotype, this mutation was detected in other affected family members with typical ADHCAI phenotypes, but the mutation was not detected in unaffected family members or normal controls (Figure 3A). The detected variant has been submitted to GenBank (MH518311, http://www.ncbi.nlm.nih.gov/WebSub/?tool=genbank).

Prediction of damaging effects

The damaging effects of this *FAM83H* mutation (p. K408X) were predicted using the online program Mutation Taste; the results predicted that this mutation would cause disease. The effects of this *FAM83H* mutation on FAM83H secondary structure were also predicted using the online program PSIPRED Protein Sequence Analysis Workbench. The results indicated structural transformations between the wild-type protein (Figure 4A) and the truncated protein (Figure 4B) in addition to the 772 amino acids missing from the C-terminus in the truncated protein.

Subcellular localization of the FAM83H mutant

As an intracellular protein with ubiquitous expression, FAM83H is normally localized to the cytoplasm under physiological conditions. Because the *FAM83H* gene (p. K408X) mutation removes 772 amino acids from the FAM83H C-terminus, this mutation might interfere with normal FAM83H protein function, including its subcellular distribution. To verify this hypothesis, we constructed a FAM83H fusion protein with a GFP tag at the N-terminus in the pEGFP-C1 vector. The c.1222A>T mutation was successfully introduced to wild-type pEGFP-FAM8H plasmid (Supplementary Figure S1). Plasmid DNA for the pEGFP-C1 vector expressing GFP, as well as pEGFP-C1 expressing wild-type or mutant FAM83H fused to GFP, was transiently transfected into RDE-SF2 cells (Figure 5A and Supplementary Figure S3A) and HEK-293T cells (Figure 5B and Supplementary Figure S3B). The transfection efficiency of HEK-293T cells is about 50–60% and that of RDE-SF2 is about 40% (Supplementary Figure S2). The GFP control was evenly distributed throughout the cytoplasm and nucleus (Figure 5I and Supplementary Figure S3I), and the wild-type FAM83H–GFP fusion protein was detected exclusively in the cytoplasm in both cell types (Figure 5II and Supplementary Figure S3II). In contrast, the K408X mutant showed a distinctly different subcellular localization from the wild-type FAM83H–GFP fusion protein. The K408X FAM83H mutant did not accumulate in the cytoplasm, as very little signal was detected; most of the mutant FAM83H–GFP fusion protein was observed in the nucleus in both cell types (Figure 5III and Supplementary Figure S3III).

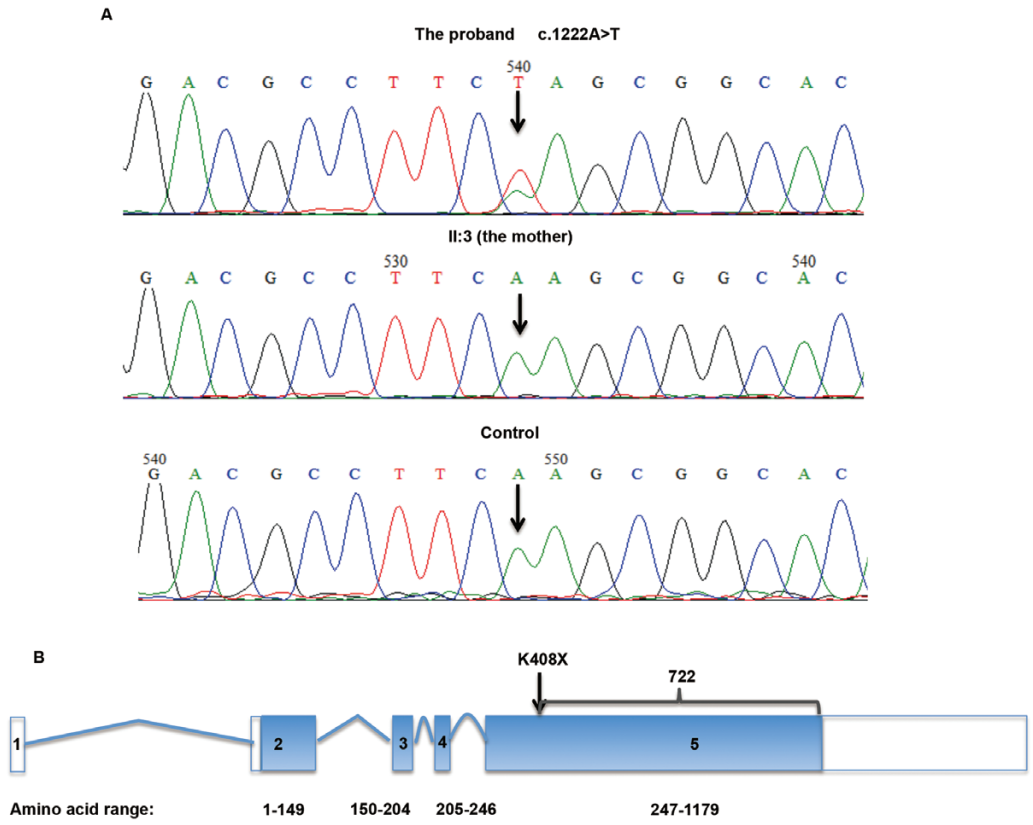

Figure 3. Mutation analysis of the *FAM83H* gene in ADHCAI patients. (**A**) A heterozygous mutation in the *FAM83H* gene identified in the proband. The mutated sequence (upper panel), the sequence for an unaffected family member (middle panel), and a normal control sequence (lower panel) are shown. Both mutated and wild-type nucleotide residues are indicated by black arrows. (**B**) Schematic presentation of the structure of the *FAM83H* gene containing the annotated mutation identified in this study. The gene diagram shows the 5 exons (boxes) and 4 introns (fold lines) of *FAM83H*. The exon coding regions are shaded. The black arrow indicates the position of the mutation.

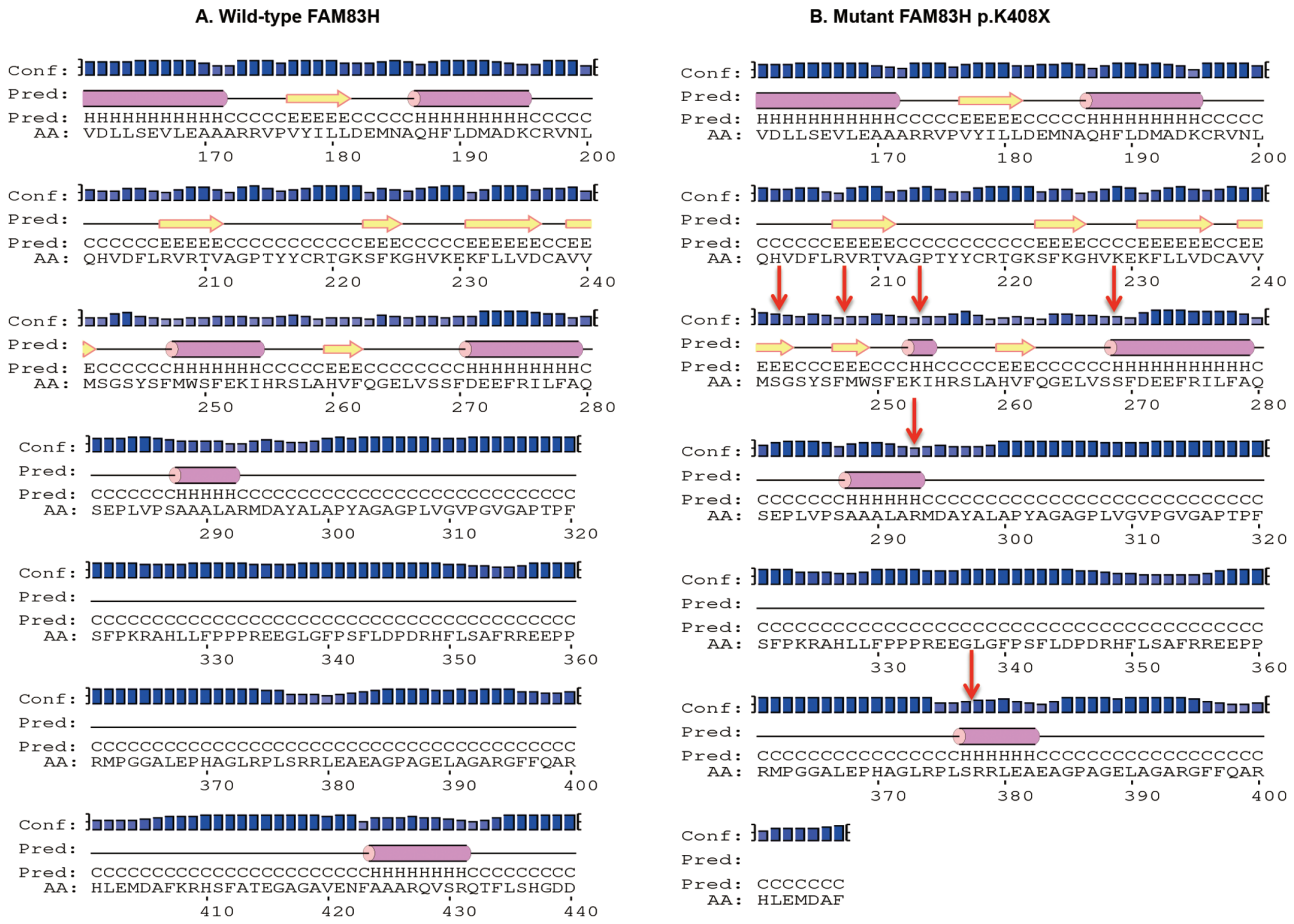

Figure 4. Predicted secondary structure of wild-type (**A**) and mutant FAM83H proteins (**B**). In addition to generating a truncated protein that is 772 amino acids shorter than wild-type, some changes between the truncated and wild-type protein are marked with red arrows starting from amino acid 242.The first 241 amino acids were nearly unchanged except for the amino acids at position 25 and 67. In the wild-type protein, the amino acid at position of 25 and 67 are a helix and coil respectively; in the mutant protein, both amino acids are switched. Pink cylinders represent the helix, yellow arrows represent the strand, and the straight lines represent the coil. Conf, the confidence of prediction. Pred, the predicted secondary structure. AA, the target sequence.

Discussion

In this study, we identified a novel *FAM83H* nonsense mutation (c.1222A>T, p. K408X) in one Chinese family in which three generations exhibited ADHCAI. Additional functional studies demonstrated that the detected mutation resulted in perturbed subcellular localization of the FAM83H protein, which might cause the typical enamel defect observed in affected patients.

ADHCAI refers to hereditary conditions that predominantly affect enamel quality with an autosomal-dominant hereditary pattern. The ADHCAI phenotype has a wide spectrum of clinical variability from localized enamel defects to extensive and generalized defects (18). In this study, the enamel of all affected family members, without exception, exhibited generalized defects, such as exfoliated enamel, exposed dark dentin with plaque accumulation and gingivitis. This finding is consistent with previous studies reporting that most affected individuals with *FAM83H* mutations have irregular, rough tooth surfaces (3). In addition, several studies have also reported that some affected individuals have a relatively mild phenotype with polished-looking dental surfaces and good gingival health (19,20). Notably, only permanent dentitions were impacted in the affected family members; however, as previously reported, primary teeth are also affected in some cases (18). Other dental abnormalities have also been reported in ADHCAI patients, such as openbite (21), crowding, crossbite and tooth impaction (5); none of these were observed in these patients.

Normal enamel is an intricate, organic–inorganic hybrid organization with hierarchical levels. First, needle-like hydroxyapatite crystals pack tightly into groups, and the organic matrix binds these crystals together (22). The crystals are then organized into the base structural unit, the enamel prism, in a species-specific manner. Finally, prisms and interprism structures assemble into prism bands across the thickness of the enamel layer. These well-organized structures endow normal enamel with superior strength and toughness (23). In this study, the normal structure of enamel, which contains typical keyhole-shaped enamel prisms and compact prism/interprism continua, was absent. Instead, irregular, poor quality enamel prisms with increased interprismatic gaps were observed in the proband. The ultrastructure enamel changes in the proband were consistent with other reports (24–26) and might be the underlying reason why the enamel of affected individuals is soft and easily exfoliated after eruption.

To date, *FAM83H* has been implicated in most ADHCAI cases and is considered to be the main causative gene for ADHCAI. The human *FAM83H* gene consists of 5 exons and encodes a non-secreted protein of 1179 amino acids (15). Human *FAM83H* exon 5 encoding aa247-1179 is relatively variable compared to exons 2–4, and all of the phosphorylation sites are located in exon 5 (27). In

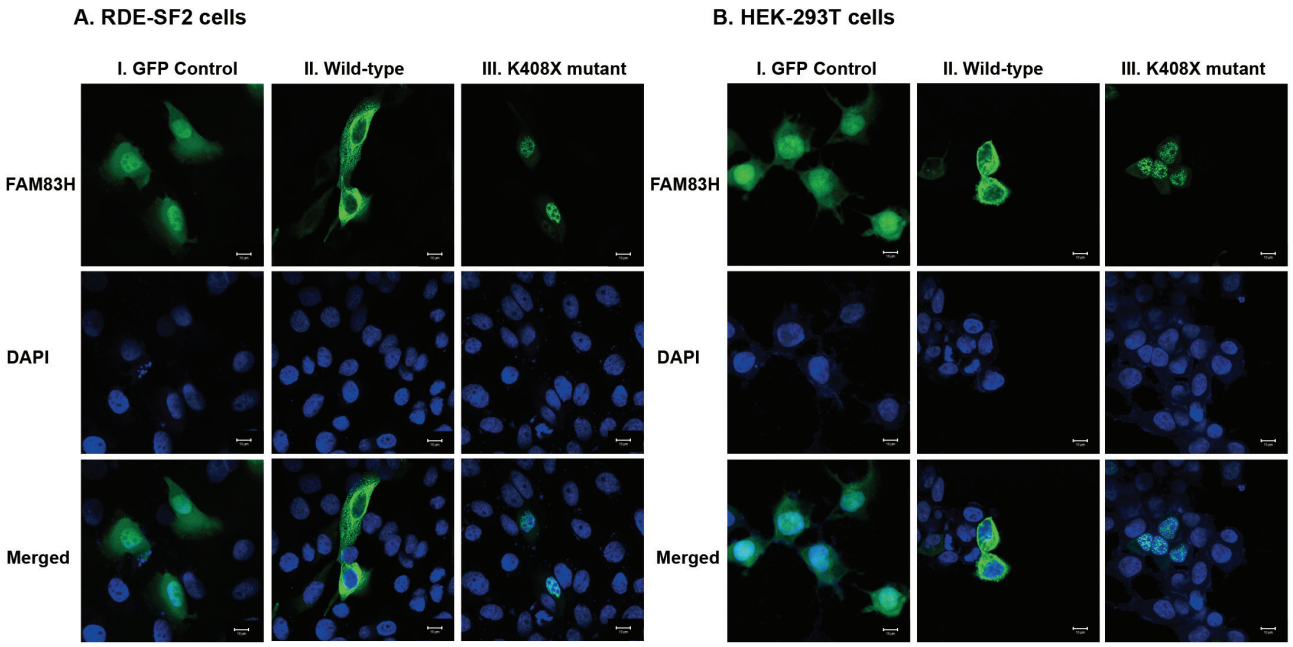

Figure 5. Subcellular localization of wild-type and mutant FAM83H-GFP fusion proteins. (**A**) RDE-SF2 cells and (**B**) HEK-293T cells were transfected with pEGFP-C1 control plasmid or pEGFP-FAM83H plasmids expressing wild-type or mutant FAM83H. Confocal micrographs (630X) show the intracellular distribution of control GFP (GFP expressed by pEGFP-C1 vector) (I), wild-type FAM83H-GFP (II) and K408X mutant FAM83H-GFP (III). (I) GFP is evenly distributed throughout the cytoplasm and nucleus. (II) Wild-type FAM83H localized exclusively to the cytoplasm, especially in the area surrounding the nucleus. (III) K408X mutant FAM83H localized mainly to the nucleus, with a faint signal in the cytoplasm. Nuclei were stained with DAPI-containing fluoroshield mounting medium. Scale bar, 10 μm.

this study, the detected mutation (p. K408X) is a nonsense mutation in exon 5 that generates a prematurely truncated protein lacking the terminal 772 amino acids. This finding is consistent with other ADHCAI studies, which report that every mutation occurs in the last exon of *FAM83H* and that most mutants truncate the protein (6,27). Although many studies have focused on the molecular mechanism of FAM83H during enamel formation, the structure and function of FAM83H have not been elucidated.

FAM83H expression is ubiquitous. In addition to expression during tooth development (28), it is also expressed in the eyes, kidney, liver, bladder and larynx (21,29). The FAM83H protein functions in the intracellular molecular transport, the regulation of cytoskeletal networks, and enamel formation (17,30). Previous studies demonstrated that the N-terminus of FAM83H interacts with casein kinase I (CK1), and the C-terminus interacts with keratins (31). In this study, the ADHCAI-causing mutation (p. K408X) generated a prematurely truncated protein missing 772 amino acids at the C-terminus. The functional studies indicated that the cytoplasmic accumulation observed for the wild-type FAM83H protein was perturbed by the K408X mutation in both RDE-SF2 cells and in HEK-293T cells, with the mutant protein localizing mainly to the nucleus. It is hypothesized that ADHCAI is caused by gain-of-function effects mediated by truncated FAM83H, which alters its subcellular localization, rather than through a dominant negative effect or by changes in FAM83H expression levels (29,30). Presumably, the truncated mutant FAM83H can interact with and alter the location of CK1, preventing normal interaction with keratins and resulting in a disassembled keratin cytoskeleton with the disappearance of keratin filaments and desmosomes (30–32). Thus, it could be inferred that mutant FAM83H disrupts the formation of desmosomes and cell-cell interactions in pre-ameloblasts, consequently interfering with the formation or function of ameloblasts in the secretory stage and leading to ADHCAI (31,32).

In conclusion, we identified a novel *FAM83H* nonsense mutation (c.1222A>T p. K408X) in one Chinese family with ADHCAI. The mutation interferes with the intracellular localization of the FAM83H protein, which might be responsible for the typical enamel defect seen in affected patients. Our results broaden the spectrum of known *FAM83H* mutations in ADHCAI individuals and contribute to our understanding of the association between mutations and the severe phenotypes observed in ADHCAI patients.

Supplementary data

Supplementary Figures S1, S2 and S3 are available at *Mutagenesis* Online.

Funding

This work was supported by the National Natural Science Foundation of China (grant number 81771053) and Project PKUSS20160105 from Peking University School and the Hospital of Stomatology Science Foundation for Young Scientists.

Acknowledgements

We are grateful to all of the participants for their contributions. We are grateful to Prof. Jan C-C. Hu (Department of Biologic and Materials Sciences, University of Michigan School of Dentistry) for providing the PEGFPC1-FAM83H plasmid and to Prof. Fukumoto S (Department of Oral Health and Development Sciences, Tohoku University Graduate School of Dentistry) for providing RDE-SF2 cells. We are also grateful to Dr. Xin Wang (Department of Pediatric Dentistry, Peking University School and Hospital of Stomatology) for technical assistance.

Conflict of interest statement: None declared.

References

1. Crawford, P. J., Aldred, M. and Bloch-Zupan, A. (2007) Amelogenesis imperfecta. *Orphanet J. Rare Dis*., 2, 17.
2. Witkop, C. J. Jr. (1988) Amelogenesis imperfecta, dentinogenesis imperfecta and dentin dysplasia revisited: problems in classification. *J. Oral Pathol*., 17, 547–553.
3. Gadhia, K., McDonald, S., Arkutu, N. and Malik, K. (2012) Amelogenesis imperfecta: an introduction. *Br. Dent. J*., 212, 377–379.
4. Sabandal, M. M. and Schäfer, E. (2016) Amelogenesis imperfecta: review of diagnostic findings and treatment concepts. *Odontology*, 104, 245–256.
5. Xin, W., Wenjun, W., Man, Q. and Yuming, Z. (2017) Novel FAM83H mutations in patients with amelogenesis imperfecta. *Sci. Rep*., 7, 6075.
6. Smith, C. E. L., Poulter, J. A., Antanaviciute, A., Kirkham, J., Brookes, S. J., Inglehearn, C. F. and Mighell, A. J. (2017) Amelogenesis imperfecta; genes, proteins, and pathways. *Front. Physiol*., 8, 435.
7. Simmer, J. P., Richardson, A. S., Hu, Y. Y., Smith, C. E. and Ching-Chun Hu, J. (2012) A post-classical theory of enamel biomineralization… and why we need one. *Int. J. Oral Sci*., 4, 129–134.
8. Moradian-Oldak, J. (2012) Protein-mediated enamel mineralization. *Front. Biosci*., 17, 1996–2023.
9. Kim, Y. J., Kim, Y. J., Kang, J., Shin, T. J., Hyun, H. K., Lee, S. H., Lee, Z. H. and Kim, J. W. (2017) A novel AMELX mutation causes hypoplastic amelogenesis imperfecta. *Arch. Oral Biol*., 76, 61–65.
10. Wang, X., Zhao, Y., Yang, Y. and Qin, M. (2015) Novel ENAM and LAMB3 mutations in Chinese families with hypoplastic amelogenesis imperfecta. *PLoS One*, 10, e0116514.
11. Poulter, J. A., Murillo, G., Brookes, S. J., Smith, C. E., Parry, D. A., Silva, S., Kirkham, J., Inglehearn, C. F. and Mighell, A. J. (2014) Deletion of ameloblastin exon 6 is associated with amelogenesis imperfecta. *Hum. Mol. Genet*., 23, 5317–5324.
12. Seymen, F., Park, J. C., Lee, K. E., *et al.* (2015) Novel MMP20 and KLK4 mutations in amelogenesis imperfecta. *J. Dent. Res*., 94, 1063–1069.
13. Hentschel, J., Tatun, D., Parkhomchuk, D., Kurth, I., Schimmel, B., Heinrich-Weltzien, R., Bertzbach, S., Peters, H. and Beetz, C. (2016) Identification of the first multi-exonic WDR72 deletion in isolated amelogenesis imperfecta, and generation of a WDR72-specific copy number screening tool. *Gene*, 590, 1–4.
14. Herzog, C. R., Reid, B. M., Seymen, F., Koruyucu, M., Tuna, E. B., Simmer, J. P. and Hu, J. C. (2015) Hypomaturation amelogenesis imperfecta caused by a novel SLC24A4 mutation. *Oral Surg. Oral Med. Oral Pathol. Oral Radiol*., 119, e77–e81.
15. Lee, S. K., Lee, K. E., Jeong, T. S., Hwang, Y. H., Kim, S., Hu, J. C., Simmer, J. P. and Kim, J. W. (2011) FAM83H mutations cause ADHCAI and alter intracellular protein localization. *J. Dent. Res*., 90, 377–381.
16. Shyu, A. B., Wilkinson, M. F. and van Hoof, A. (2008) Messenger RNA regulation: to translate or to degrade. *EMBO J*., 27, 471–481.
17. Ding, Y., Estrella, M. R., Hu, Y. Y., Chan, H. L., Zhang, H. D., Kim, J. W., Simmer, J. P. and Hu, J. C. (2009) Fam83h is associated with intracellular vesicles and ADHCAI. *J. Dent. Res*., 88, 991–996.
18. Wright, J. T., Frazier-Bowers, S., Simmons, D., Alexander, K., Crawford, P., Han, S. T., Hart, P. S. and Hart, T. C. (2009) Phenotypic variation in FAM83H-associated amelogenesis imperfecta. *J. Dent. Res*., 88, 356–360.
19. Hart, P. S., Becerik, S., Cogulu, D., Emingil, G., Ozdemir-Ozenen, D., Han, S. T., Sulima, P. P., Firatli, E. and Hart, T. C. (2009) Novel FAM83H mutations in Turkish families with autosomal dominant hypocalcified amelogenesis imperfecta. *Clin. Genet*., 75, 401–404.
20. Song, Y. L., Wang, C. N., Zhang, C. Z., Yang, K. and Bian, Z. (2012) Molecular characterization of amelogenesis imperfecta in Chinese patients. *Cells. Tissues. Organs*, 196, 271–279.
21. Kim, J. W., Lee, S. K., Lee, Z. H., *et al.* (2008) FAM83H mutations in families with autosomal-dominant hypocalcified amelogenesis imperfecta. *Am. J. Hum. Genet*., 82, 489–494.
22. Jiang, T., Ma, X., Wang, Z., Tong, H., Hu, J. and Wang, Y. (2008) Beneficial effects of hydroxyapatite on enamel subjected to 30% hydrogen peroxide. *J. Dent*., 36, 907–914.
23. He, L. H. and Swain, M. V. (2007) Enamel - a "metallic-like" deformable biocomposite. *J. Dent*., 35, 431–437.
24. Zhang, C., Song, Y. and Bian, Z. (2015) Ultrastructural analysis of the teeth affected by amelogenesis imperfecta resulting from FAM83H mutations and review of the literature. *Oral Surg. Oral Med. Oral Pathol. Oral Radiol*., 119, e69–e76.
25. El-Sayed, W., Shore, R. C., Parry, D. A., Inglehearn, C. F. and Mighell, A. J. (2010) Ultrastructural analyses of deciduous teeth affected by hypocalcified amelogenesis imperfecta from a family with a novel Y458X FAM83H nonsense mutation. *Cells. Tissues. Organs*, 191, 235–239.
26. Belcheva, A. B., Philipov, I. A. and Tomov, G. T. (2016) Scanning electron microscopy of enamel and dentin of teeth with hypocalcified amelogenesis imperfecta. *Folia Med. (Plovdiv)*., 58, 54–59.
27. Huang, W., Yang, M., Wang, C. and Song, Y. (2017) Evolutionary analysis of FAM83H in vertebrates. *PLoS One*, 12, e0180360.
28. Lee, M. J., Lee, S. K., Lee, K. E., Kang, H. Y., Jung, H. S. and Kim, J. W. (2009) Expression patterns of the Fam83h gene during murine tooth development. *Arch. Oral Biol*., 54, 846–850.
29. Kweon, Y. S., Lee, K. E., Ko, J., Hu, J. C., Simmer, J. P. and Kim, J. W. (2013) Effects of Fam83h overexpression on enamel and dentine formation. *Arch. Oral Biol*., 58, 1148–1154.
30. Wang, S. K., Hu, Y., Yang, J., *et al.* (2016) Fam83h null mice support a neomorphic mechanism for human ADHCAI. *Mol. Genet. Genomic Med*., 4, 46–67.
31. Kuga, T., Kume, H., Kawasaki, N., *et al.* (2013) A novel mechanism of keratin cytoskeleton organization through casein kinase Iα and FAM83H in colorectal cancer. *J. Cell Sci*., 126, 4721–4731.
32. Kuga, T., Sasaki, M., Mikami, T., *et al.* (2016) FAM83H and casein kinase I regulate the organization of the keratin cytoskeleton and formation of desmosomes. *Sci. Rep*., 6, 26557.